

## AugerPrime - The upgrade of the Pierre Auger Observatory

Jarosław Stasielak for the Pierre Auger Collaboration<sup>\*†‡</sup>  
*Institute of Nuclear Physics Polish Academy of Sciences*  
*Radzikowskiego 152, 31-342 Kraków, Poland*  
*jaroslaw.stasielak@ifj.edu.pl*

Received Day Month Year  
 Revised Day Month Year

Ultra-high-energy cosmic rays (UHECRs) are studied with giant ground-based detector systems recording extensive air showers, induced by cosmic ray particles in the atmosphere. Research at the Pierre Auger Observatory - the largest of such detectors ever built – largely contributed to a number of breakthroughs and dramatically advanced our understanding of UHECRs. Nonetheless, the results so far are still inconclusive as neither have the sources of these most energetic particles known in the Universe been determined, nor has the origin of the unambiguously established cosmic ray flux suppression above 40 EeV been fully understood. At the same time, precise measurements of the muon component of the extensive air showers on the ground show discrepancies with the predictions of hadronic interaction models. The explanation of these puzzles, which are closely related to each other, is one of the most important goals of modern astrophysics.

The results obtained by the Pierre Auger Observatory indicate that further advances in understanding UHECRs require an improvement of the measuring capabilities of existing detectors, where the key feature is a superior separation of the muonic and electromagnetic components of air showers. AugerPrime, the ongoing upgrade of the Pierre Auger Observatory has been designed for this task. The main objective of the AugerPrime is to enhance the sensitivity of our analyses to the masses of cosmic rays, which will help to elucidate the origin of the UHECRs. In this paper we overview the main features of the AugerPrime design, its current status, and discuss the goals and potential capabilities of the upgraded Observatory.

*Keywords:* ultra-high energy cosmic rays; extensive air showers; AugerPrime.

PACS numbers: 98.70.Sa, 95.55.Vj, 95.85.Ry

### 1. Introduction

The Pierre Auger Observatory,<sup>1</sup> located on a vast, high plain in Argentina, is the world's largest detection system for the observation of ultra-high-energy cosmic rays (UHECRs) (i.e. cosmic rays with energies above 1 EeV =  $10^{18}$  eV). Detection of these most energetic particles observed in the Universe, is feasible only indirectly,

<sup>\*</sup>Full author list: [http://www.auger.org/archive/authors\\_2020\\_09.html](http://www.auger.org/archive/authors_2020_09.html)

<sup>†</sup>Observatorio Pierre Auger, Av. San Martín Norte 304, 5613 Malargue

<sup>‡</sup>auger\_spokespersons@fnal.gov

through observations of the so-called extensive air showers (EAS), i.e. cascades of secondary particles initiated high in the atmosphere by incoming cosmic ray particles. The air shower takes the form of a thin disk ( $\sim 10$  m), made up of a huge number of particles, moving with the speed of light towards the ground. The disk is slightly bent, with particles far from its central part staying a little behind. The diameter of the disk, as well as the number of particles within the cascade, change with its development in the atmosphere, and can reach several kilometers and several billions, respectively. Cascade grows, reaches a maximum and then dies out. It can be divided into three components, namely the hadronic, electromagnetic and muonic, where the last two components dominate.

The main facilities of the Pierre Auger Observatory are the Surface Detector (SD),<sup>2</sup> an array of 1661 water-Cherenkov detectors (WCD) deployed over an area of 3000 km<sup>2</sup>, measuring the lateral distribution of particles in a shower at ground level, and the Fluorescence Detector (FD),<sup>3</sup> with 27 telescopes, overlooking the atmosphere above the SD array. The FD records the fluorescence light generated in the atmosphere by the charged particles of shower through excitation of N<sub>2</sub> molecules, measuring the longitudinal development of EAS in the atmosphere. The Auger Observatory is a hybrid detector utilizing simultaneously both of these complementary techniques to make measurements of extensive air showers more precise. The FD operates only during clear, moonless nights, which limits its duty cycle to  $\sim 13\%$ . In contrast, the SD array works continuously, regardless of weather conditions. Additionally, 7 underground muon counting stations<sup>4,5</sup> and a several km<sup>2</sup> array of radio antennas<sup>6</sup> measuring the radio signal emitted by air showers, provide an extra information, complementing the SD and FD data.

Research at the Pierre Auger Observatory largely contributed to a number of breakthroughs and dramatically advanced our understanding of UHECRs. As an example, the suppression of the cosmic ray flux above  $\sim 40$  EeV has been established unambiguously<sup>7,8</sup> (see Fig. 1, top panel). Another significant result was the observation of a dipolar large-scale anisotropy in the arrival directions of cosmic rays above 8 EeV,<sup>9,10</sup> indicating that they are indeed of extragalactic origin. With these advances, however, new, more specific questions have been revealed; still, the sources of these most energetic particles known in the Universe remain to be identified and the origin of the flux suppression has to be fully understood. At the same time, precise measurements of the muon component of extensive air showers on the ground show discrepancies with the predictions of hadronic interaction models.<sup>11–14</sup> The explanation of these puzzles, which are closely related to each other, is one of the most important goals of modern astrophysics.

The suppression of the cosmic ray flux was predicted more than 50 years ago as a result of the particle energy losses en route to Earth due to the pion photo-production on the cosmic microwave background and is known as the Greisen-Zatsepin-Kuzmin (GZK) cutoff.<sup>16,17</sup> In such a scenario, cosmic rays should be dominated by protons at the flux suppression region. However, the experimental data

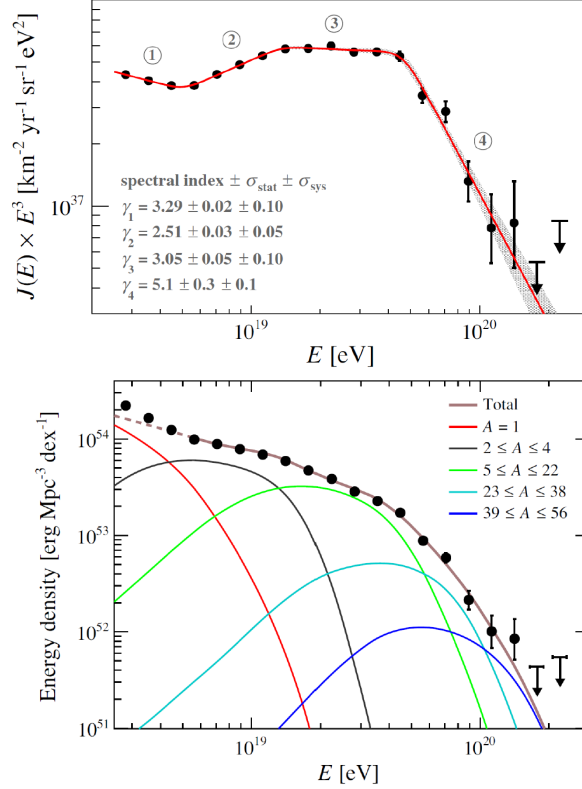


Fig. 1. Top panel: The Auger energy spectrum of UHECRs scaled by  $E^3$ . Shown are a broken power-law fit (red line) and spectral indexes of the fit for each of the energy intervals. The shaded band indicates the 90% confidence level of the fit. The suppression of the cosmic ray flux at  $\sim 40$  EeV is clearly visible; Bottom panel: Energy density of different mass components best reproducing the Auger data. The plot is obtained by simultaneously fitting the energy spectrum above 5 EeV and the composition-sensitive data (the distributions of both the atmospheric depths of maximum of shower development,  $X_{\text{max}}$ , and their fluctuations,  $\sigma(X_{\text{max}})$ ). See Ref. 15 for details. The mass number of nuclei is denoted by  $A$ . The mass composition is dominated by heavy nuclei at the highest energies which is characteristic for the maximum rigidity scenario. Figures taken from Ref. 7.

on the cosmic ray composition collected in the Pierre Auger Observatory show that the fraction of protons seems to dominate only at the energies of a few EeV, and is successively replaced by heavier elements at higher energies.<sup>18–25</sup> This feature can be interpreted as a manifestation of the limit of the particle acceleration at the source, with the maximum energy proportional to the particle charge (it is the so-called maximum rigidity scenario). In fact, the energy spectrum and the composition data are better reproduced by a simple astrophysical model of the UHECR sources in the latter case<sup>7,15</sup> (see Fig. 1, bottom panel). The same scenario is also supported by the lack of observation of ultra-high-energy neutrinos (which should be produced as a result of the GZK effect) – recently more stringent upper limits

for their fluxes have been set.<sup>26</sup> The GZK effect and the maximum rigidity scenario do not exclude each other, and the spectrum of cosmic rays observed may be the result of a combination of different effects. However, with the observations collected so far, we are not able to determine which model is correct. Composition determination of UHECRs (preferably on an event-by-event basis) at energies above the flux suppression region ( $> 40$  EeV) is the key to resolve this issue.

Another puzzle is a weak correlation of cosmic rays with the distribution of nearby galaxies observed above 50 EeV,<sup>9, 10, 27, 28</sup> which could be explained by  $\sim 10\%$  fraction of protons at these energies. The ultra-high-energy protons should be deflected in the intergalactic magnetic field by only several degrees, which would enable tracking back to their sources. In contrast, more massive nuclei would erase any detectable correlations. However, extrapolating the composition results to the highest energies, we conclude that the protons constitute much lower fraction of the cosmic ray flux than expected. It is again understandable that measurement of cosmic ray composition at energies above 50 EeV is crucial for further progress in this investigation. The ability to identify primary protons in the observed UHECRs would provide a way to reliably point to the sources, and thus possibly establish the proton astronomy.

Determination of cosmic ray composition is closely related to air shower physics and thus relies heavily on the hadronic interaction models. Any inaccuracies related to extrapolation of their properties, from energies at which they are measured at terrestrial particle accelerators, to the ultra-high energies may influence the interpretation of the mass-sensitive data. The number of muons seen experimentally in air showers is 30-60% larger than the numbers obtained in the simulations.<sup>11-14</sup> This indicates a poor understanding of hadronic interaction models at the highest energies and shows that further advances require an improvement of the measuring capabilities of existing detectors, where the key feature is a superior separation of the muonic and electromagnetic components. This will simultaneously help us with the mass composition study.

The ongoing upgrade of the Pierre Auger Observatory, called AugerPrime<sup>29</sup> (Primary cosmic Ray Identification with Muons and Electrons), has been designed for this task. It will enhance our ability to measure the mass composition of cosmic rays above  $\sim 10^{19.5}$  eV (possibly on event-by-event basis), providing information for more accurate analysis of air shower development and allowing:

- to elucidate the mass composition and the origin of the flux suppression at the highest energies, i.e. the differentiation between the GZK and maximum rigidity scenarios.
- to reach a sensitivity to a contribution of protons as small as 10% in the flux suppression region, thus evaluating the possible existence of a small fraction of protons at these energies and assessing the feasibility of charged particle astronomy.
- to improve our knowledge about hadronic interactions: increasing the ac-

curacy of existing models extrapolated to the extreme observed energies.

As a part of the upgrade, the SD water-Cherenkov tanks will be equipped with additional scintillator (SSD) and radio detector (RD) units. In addition, new, faster and more precise acquisition electronics along with a small PMT will be installed in all surface detectors. It is also planned to relax the restrictions on the FD operations, which will increase its duty cycle. Finally, the AugerPrime will be supplemented with the upgraded Underground Muon Detector (UMD).

## 2. New Surface Scintillator Detector (SSD)

To use the full statistics of the SD data to analyze the composition of cosmic rays, the Pierre Auger Collaboration has made the decision to upgrade the SD by placing surface scintillator detectors on top of almost all (beside stations located at the outskirts of the array) of the existing SD water-Cherenkov detectors.<sup>29</sup> The plastic scintillators and water-Cherenkov detectors responses to shower components are different. Muons have larger energy deposits in water than electromagnetic particles, and at the same time both of these components deposit on average the same amount of energy in the scintillator. In this sense, the WCD is more sensitive to muons, whereas the SSD to the electromagnetic component of shower. Given the different sensitivities of scintillators and water-Cherenkov detectors to electrons, photons, and muons of extensive air shower, the combination of measurements from these two detector types will provide muon content information (on event-by-event basis), which is vital for cosmic ray mass composition studies and improved energy determination. The disentangling electromagnetic and muonic components at ground is the best available method for the mass composition measurements, when the direct optical observation of the depth of shower maximum,  $X_{\text{max}}$ , by the FD is not possible (which is the most reliable method of mass composition determination, but very limited at the highest energies due to the small FD duty cycle). Comparing the signals from the two detectors will allow us to separate the contributions from muons and electromagnetic particles with a precision unavailable before. The Observatory upgrade will allow measurements of the composition of cosmic rays at energies above  $\sim 40$  EeV, i.e. above the flux suppression region, which have been unattainable until now.

A complementary measurement of shower particles is provided by a plastic scintillator plane above the existing water-Cherenkov detectors. The design of the SSD is simple, reliable and the SSD modules can be easily deployed over the full  $3000 \text{ km}^2$  area of the Surface Detector. The SSD module is composed of a light-tight, water-proof, aluminium enclosure of  $3.8 \text{ m} \times 1.3 \text{ m}$ , housing 48 scintillator bars made of extruded polystyrene, which are the active part of the detector. They are placed symmetrically on both sides of the detector. Each scintillator bar of dimension  $160 \text{ cm} \times 5 \text{ cm} \times 1 \text{ cm}$ , with an outer reflective layer of  $\text{TiO}_2$ , has two co-extruded channels through which wavelength-shifting optical fibers are routed. The fibers are laid in a U-shape configuration that maximizes light yield and uniformity. All

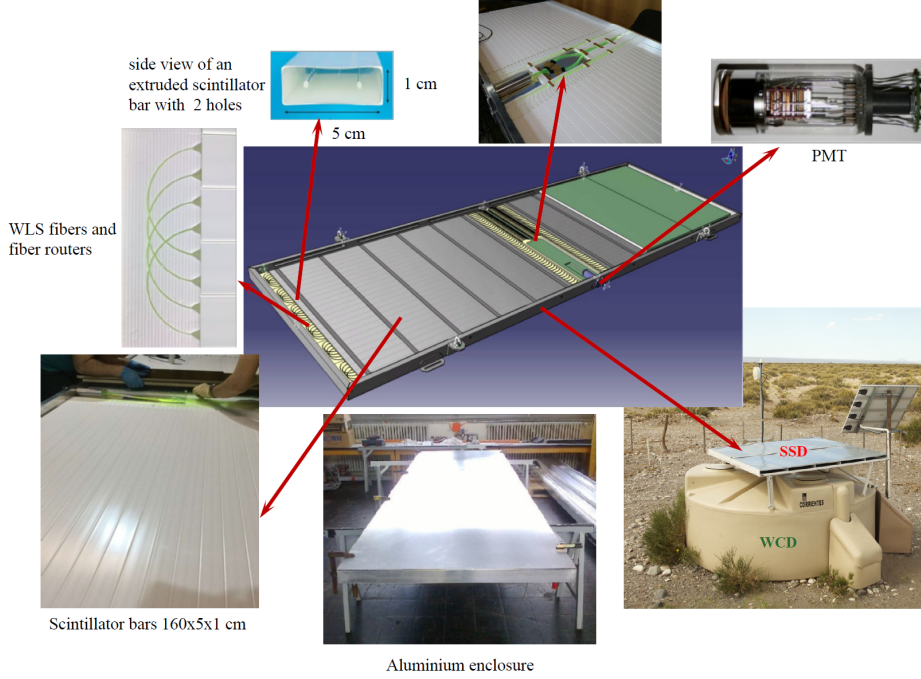


Fig. 2. Layout of the surface scintillator detector (SSD) module. See description in the text.

ends of the fibers, collecting the scintillation light produced by the shower particles, are bundled towards a single photomultiplier tube (PMT) located in the central part of the module. The design of the SSD was tested and validated in the Pierre Auger Observatory. The layout of an SSD module and its placement above a WCD detector is shown in Fig. 2.

The assembly of the SSD modules has been distributed among several institutions of the Pierre Auger Collaboration. The large-scale production started in 2017, and it is now completed. All SSDs were tested at each construction site upon completion, exploiting atmospheric muon tomography to measure the minimum ionizing particle (MIP) as well as to check the SSD modules uniformity.<sup>30</sup> The test measurements allow identification of both MIPs and single photoelectrons (SPEs) signals (see Fig. 3, left panel). The mean charge of the MIP and SPE is determined by fitting peaks to the histograms obtained during the tests. The ratio of these values reflects the overall efficiency of SSD (efficiency of the key detector components at generating, collecting and transmitting the light). An example distribution of the MIP to SPE ratio obtained from one institution is shown in the right panel of Fig. 3.

The shape of the MIPs peak (Fig. 3, left panel) tests the uniformity of SSD response over its active area. A deformation of this peak would indicate that a large part of the detector is deficient. More detailed tests of selected SSD modules, based on a different method, showed that signals from individual scintillator bars deviate

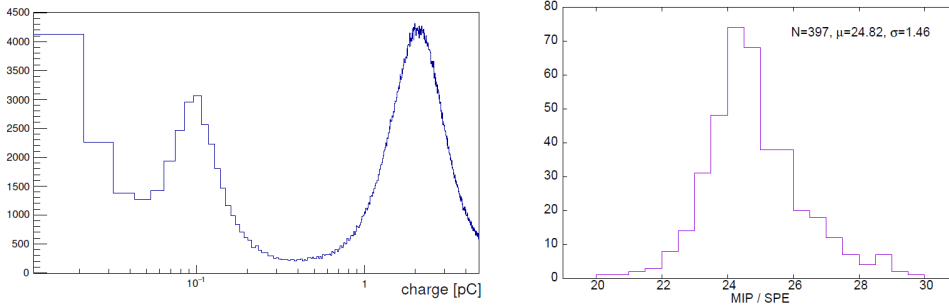


Fig. 3. Left panel: Histogram of signals recorded in a test measurement of one SSD module. The peaks corresponding to electronics noise, SPEs and MIPs are shown from left to right, respectively; Right panel: Distribution of the MIP to SPE ratio for SSDs made in one of the assembly sites. Figures taken from Ref. 30.

by no more than 10% from the average signal.

As a part of the Auger upgrade, new, faster and more precise acquisition electronics will be installed in all SD stations, thus replacing the so-called Unified Board (UB) with an Upgraded one (UUB).<sup>31</sup> The UUB will enable to simultaneously process signals from the water-Cherenkov detectors, surface scintillator detectors, radio detectors, and underground moun detectors and will increase the data quality by providing:

- faster sampling of ADC traces (40 MHz  $\rightarrow$  120 MHz) and more precise absolute timing accuracy from new GPS receivers (12 ns  $\rightarrow$  4 ns), which is better suited for counting muons (distinguishing sharp, large muon pulses close in time)
- faster data processing and more sophisticated local trigger (more powerful processor and FPGA)
- larger dynamic range (10 bits  $\rightarrow$  12 bits)
- more FADC channels (6  $\rightarrow$  10)
- improvement in the calibration and monitoring capabilities
- backwards-compatibility with the old design (similar power consumption, hardware interfaces, etc.).

Moreover, each WCD will be quipped with an additional small photomultiplier (SPMT), with a low-gain, and an active area of about 1% of the currently working large PMT (LPMT). The SPMT will register large pulses from very close showers that saturate the LPMT signal, enlarging the dynamic range of the detector by a factor of 32 (up to  $\sim 20\,000$  VEM, the energy equal of Vertical Equivalent Muon). This is demonstrated in Fig. 4, which shows distributions of charge measured in one of the upgraded SD stations (left panel) and the correlation between the signals in one of the WCD and in the corresponding SSD (right panel). Signals are expressed in physical units – VEM for the WCD and MIP for the SSD. The dynamic range

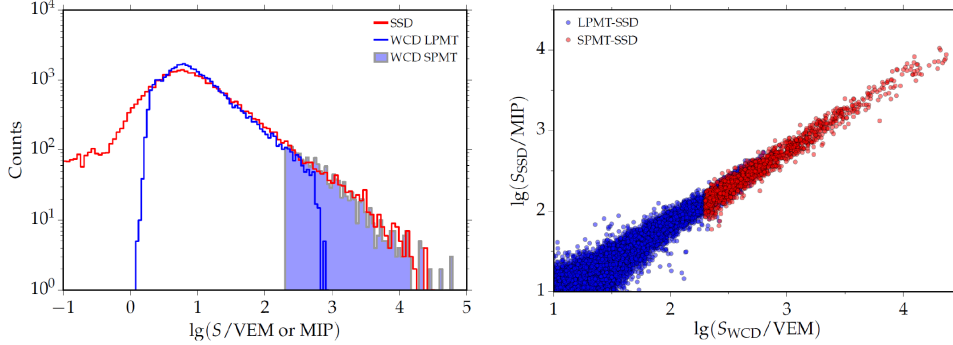


Fig. 4. Left panel: Distributions of charge measured in one of the upgraded SD stations by SSD (red) and WCD (blue) signals. The filled histogram shows signals from the small PMT; Right panel: Correlation between SSD and WCD signals (measured in MIP and VEM respectively) using the large PMTs (blue) and the small PMT (red).

in the upgraded SD is nicely covered by the LPMTs up to the saturation and then extended to the highest SSD signals by the SPMT. Larger dynamic range will allow for determination of the particle densities closer to the shower core, e.g. down to 250 m for a 10 EeV shower.

An Engineering Array consisting of the 12 upgraded SD stations has been collecting data since 2016. In addition, a pre-production SSD array of 77 stations is fully operational since March 2019. The upgraded stations operate with good stability. The results obtained by these arrays are very encouraging. They demonstrate the quality of the new detectors and the physics potential of the upgraded SD array. More than 1000 SSD modules (out of  $\sim 1500$ ) have been already deployed in the field. Further deployment is in progress and will be finished soon.

### 3. The Radio Upgrade

Extensive air showers consist of charged particles that undergo acceleration in the atmosphere and therefore they are a source of radio emission in the frequency range of tens MHz up to several GHz.<sup>32</sup> The radio emission mainly arises due to the geomagnetic deflection of the electrons and positrons in the shower, however, the Askaryan effect related to the time variation of the net charge excess in the shower front, is also important. For several years now, the Auger Engineering Radio Array (AERA),<sup>33</sup> an array of more than 150 radio detector stations covering an area of about 17 km<sup>2</sup>, has been successfully recording the radio emission of air showers. To fully utilise detection capabilities of the radio technique, it was decided to extend the existing Radio Detector to the entire SD array. Thus, each water-Cherenkov detector of the SD array will be equipped both with an SSD and a radio antenna, forming the largest radio array in the world, covering 3000 km<sup>2</sup>. An already upgraded SD station, with a scintillator detector and a radio antenna installed is shown in Fig. 5 (left panel).



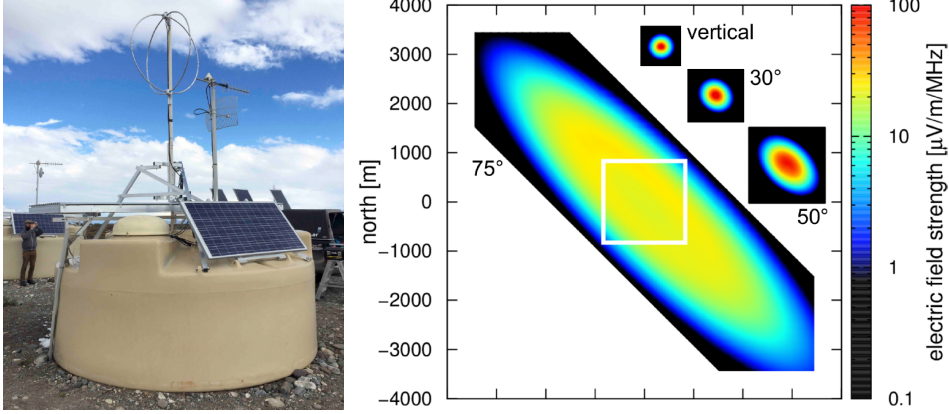


Fig. 5. Left panel: An upgraded SD station, including the new scintillator detector and new radio antenna on top of the Water-Cherenkov detector; Right panel: Footprint of the shower radio emission on the ground in the 30-80 MHz frequency band as simulated with CoREAS.<sup>34</sup> While the radio emission footprint is small for air showers with zenith angles up to  $\approx 60^\circ$ , it becomes very large for inclined showers with zenith angles of  $70^\circ$  or larger. The white rectangle characterizes the size of the 50° inset. Figure taken from Ref. 35.

The radio array will be composed of the short aperiodic loaded loop antennas (SALLAs) detecting the radio emission from air showers in the frequency range of 30 to 80 MHz. The SALLA has been developed to provide a minimal design that fulfills the need for both ultra-wide band sensitivity and low costs for production and maintenance of the antenna in a large-scale radio detector. The compact structure of the SALLA makes the antenna robust and easy to manufacture. Its sensitivity is a flat function of radio frequency. The antenna measures along two polarization directions, oriented orthogonal to each other.

The new Radio Detector will operate together with the upgraded SD, forming a unique setup to measure the properties of air showers. The size of the footprint of radio emission on the ground increases with the shower zenith angle (see Fig. 5, right panel), covering areas of the order of  $100 \text{ km}^2$  for very inclined showers. Due to the size of the radio footprint, observations of air showers by a sparse antenna array with 1.5 km spacing is only feasible for inclined showers, i.e. those with zenith angles larger than  $\sim 60^\circ$ . The RD will be useful for studying inclined showers, for which the SSD efficiency drops due to geometrical reasons. Supplementing the water-Cherenkov stations with both SSD and RD detectors will extend the shower measurement capabilities over the full angular range. The combination of WCD and RD will be used to measure the ratio of the electromagnetic energy content and the number of muons (providing separation of the electromagnetic and muonic components) for inclined air showers at the highest energies. It is similar to what has previously been done with the combination of WCD and Fluorescence Detector, however, with much higher event statistics due to the 100% duty cycle of the Radio Detector.

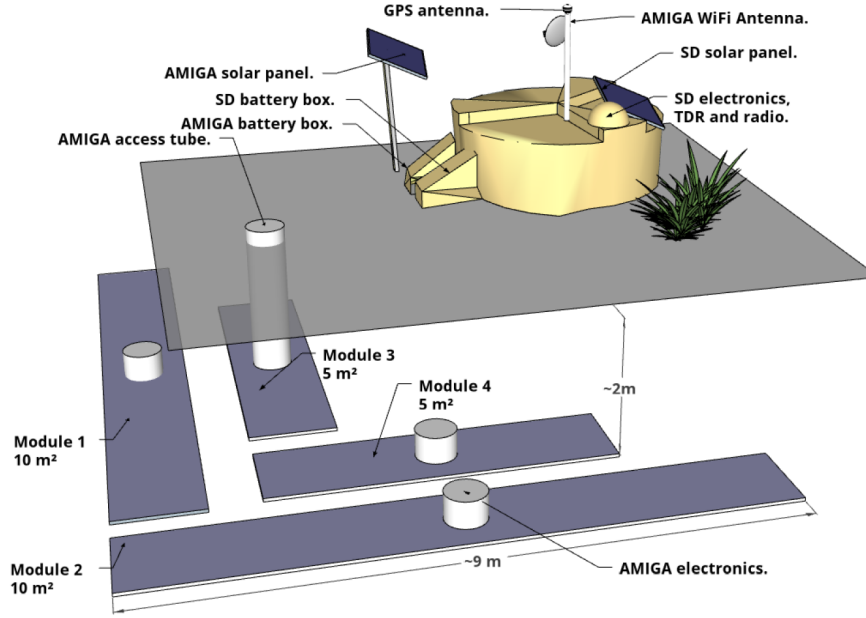


Fig. 6. Underground muon detector general overview. Both surface and underground detector, are shown in their arrangement during the prototype phase. In the final design, the  $30 \text{ m}^2$  detector is splitted into three  $10 \text{ m}^2$  modules.

The Auger Radio Detector is a natural next step towards future cosmic-ray experiments. It will allow to evaluate the detector technology, establish reconstruction methods, and study the physics performance of huge sparse radio arrays.

#### 4. Upgrade of the Underground Muon Detector

The most direct measurement of the muon content of air showers is provided by the underground detectors, buried under a several-meter layer of soil, that are sufficiently shielded against the electromagnetic component. It would be impractical, however, to install such detector under all of the 1661 SD stations, that are distributed over a large area, with difficult access in some parts. Therefore, it was decided to build a smaller array by extending the existing Underground Muon Detector, currently consisting of 7 AMIGA<sup>a</sup> muon stations,<sup>4,5</sup> to an area of the SD Infill, i.e. a small WCD array designed to extend the energy range of shower measurements of the Auger Observatory down to  $\sim 10^{17} \text{ eV}$ .

Each SD station of the Infill will be supplemented with the AMIGA muon detector (UMD station), consisting of 3 scintillator modules of  $10 \text{ m}^2$  area, buried at a depth of 2.3 m, at a distance large enough from the water tank to avoid shadow-

<sup>a</sup>Auger Muons and Infill for the Ground Array



Fig. 7. Left panel: Scintillator module. The black optical connector concentrates the 64 optical fibers coming from the 32 scintillator bars at each side of the detector; Right panel: Deployment of an AMIGA muon detector. The shown service-tubes are to provide access to the electronics for development and maintenance purposes.

ing (to guarantee uniform shielding), see Fig. 6. The scintillator module is made of 64 scintillator strips (4 m long, 4.1 cm wide, 1 cm thick). Light collected at each strip is guided, using wavelength shifting fibers, towards a 64 channel silicon photo sensor<sup>36</sup> located in the middle of the module (see Fig. 7, left panel). The segmented structure of the scintillator module allows for direct counting of muons. The Underground Muon Detector will consist of 61 stations deployed on a 750 m triangular grid of the SD Infill, instrumenting its entire area of 23.5 km<sup>2</sup>. Deployment of an UMD detector is shown in Fig. 7 (right panel).

Comparing the measurements obtained by the surface detectors with those from a small array of underground muon detectors should significantly improve the accuracy of the AugerPrime results. The UMD will provide important direct muon measurements of a sub-sample of showers, along with their time structure. It will be used for verification and fine-tuning of the methods used to extract muon information from the SSD and WCD measurements.

## 5. Increase of the FD up-time

Out of the composition-sensitive observables, the atmospheric depth of maximum of shower development,  $X_{\max}$ , is currently the one with the smallest systematic uncertainties and the most direct link to the mass distribution of the primary particles.<sup>37,38</sup> It is best determined from the longitudinal profile of the shower, recorded using the fluorescence telescopes. Unfortunately, the standard Fluorescence Detector operation is performed only during nights with a low sky background, i.e. nights with the illuminated fraction of the Moon below 70%. The data acquisition is performed during astronomical nights (when the Sun is more than 18° below the horizon) and in good weather conditions. These all together inevitably limit the FD's duty cycle to ~13%. Due to the small duty cycle of the FD and a rapid decrease of the cosmic ray flux with energy, the sufficient statistics of the recorded FD events,



Fig. 8. Left panel: Test of data acquisition with reduced PMTs gain performed at full moon. Shown is the FD building with open shutters during the test. The full Moon and Jupiter are clearly visible on the sky above the building; Right panel: One of the FD remote-control rooms of the Auger Observatory.

with direct optical observations of the shower maximum  $X_{\max}$ , cover only energies up to  $\sim 40$  EeV, i.e. just below the flux suppression region.

Hence the idea to extend the operation time of the fluorescence detector and to collect data even when the night sky background is high. The FD up-time can be increased if the restrictions on the illuminated fraction of the moon and its presence above the horizon are relaxed, and by including the astronomical twilight for the observation time (i.e. the time intervals when the Sun is between  $12^\circ$  and  $18^\circ$  below the horizon). No changes in the FD hardware are needed for this purpose.

To operate the FD during nights when diffuse moonlight increases night sky background, it is necessary to decrease the gain of photomultipliers installed in the FD camera to avoid their damage. This in turn leads to degradation of the quality of collected data (especially for low energy events). However, analyses performed indicate that the most energetic events can be measured even with the background increased by a factor of 10 (with appropriately reduced PMTs gain), while still keeping almost 100% selection efficiency as well as a good energy and  $X_{\max}$  resolutions. This will allow to increase the FD duty cycle to  $\sim 25\%$  and thus almost double the rate of collecting good-quality hybrid data above the energy of  $\sim 40$  EeV, providing (by increasing statistics) the valuable mass composition measurements in the flux suppression region.

The FD PMTs have been already extensively tested at the nominal and lowered gain levels in a dark chamber, showing a linear response in the considered gain range. Moreover, a dedicated test at the Pierre Auger Observatory was performed: in one of the telescopes the PMTs gain was reduced by a factor of 10, i.e. from the nominal gain of 50 000 to 5000, and showers with higher energies could be easily recorded at full moon (see Fig. 8, left panel).

The extension of the FD up-time will result in an increase of the number and length of FD data acquisition shifts. A recently developed technique of remote shifts, which uses remote-control rooms at distant institutions that are connected to the Observatory via the Internet network, will significantly help in FD operation.

Currently, there are several remote-control rooms being operational in the Auger Collaboration. One of such rooms is shown in Fig. 8 (right panel).

The extended mode of the FD operation will allow us to double the rate of accumulating high-quality hybrid data (with directly measured  $X_{\max}$ ) at the highest energies, providing the cross-check with the mass composition study performed by the upgraded Surface Detector.

## 6. Performance of the AugerPrime Detector

One of the key questions concerning the physics reach of the AugerPrime is its sensitivity for mass composition, in particular the feasibility to detect a fraction of protons as small as 10% at the highest energies. This is not easy to demonstrate, since we do not know what composition to expect. Nevertheless, one can select two exemplary benchmark models of cosmic ray composition for comparison to address this problem. One of them is a maximum rigidity scenario ("scenario 1"), corresponding to the best fit to the Auger cosmic ray flux and mass composition data for  $E > 10^{18.7}$  eV.<sup>15</sup> The second scenario ("scenario 1p") is constructed on the basis of the first one by artificially adding a contribution of 10% protons to it. Two sets of mock data with a cosmic ray mass composition corresponding to these scenarios were generated and used to simulate the response of the upgraded Surface Detector (not including the radio detector). As a result, using the information from the SSD combined with the WCD data, the distributions of depth of shower maximum ( $X_{\max}$ , measured indirectly), relative number of muons ( $R_{\mu,38}$ ), and their fluctuations ( $\text{RMS}(X_{\max})$  and  $\text{RMS}(R_{\mu,38})$ ) have been obtained for both

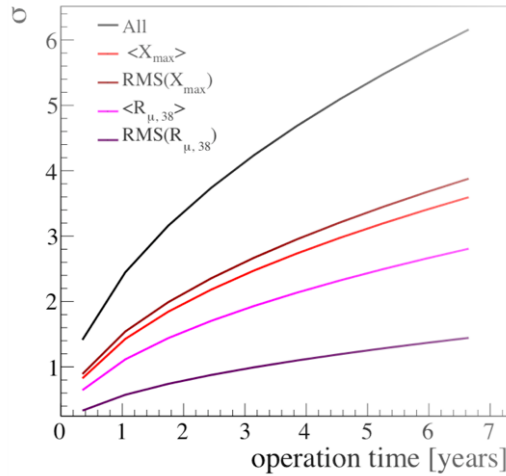


Fig. 9. Significance of distinguishing between scenarios "1p" and "1" (i.e. between maximum rigidity scenario with and without additional 10% fraction of protons, respectively) as a function of the operation time of AugerPrime.

sample datasets.

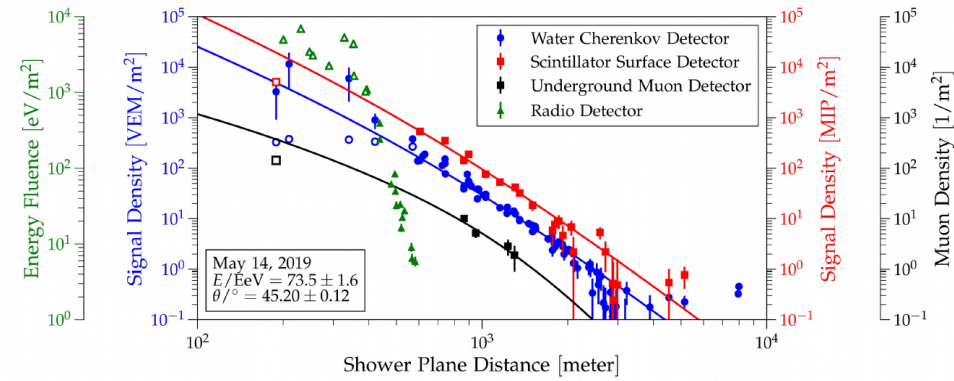


Fig. 10. An example of a real multi-hybrid event, i.e. event observed simultaneously by various detectors of the Pierre Auger Observatory. Shown are lateral distributions of signals measured by WCD (blue), SSD (red), UMD (black), and RD (green), as a function of the distance to the shower core.

The difference  $\sigma$  between the means of these distributions as obtained from the two scenarios ("1" and "1p") divided by the statistical uncertainty as a function of the operation time of the upgraded detector is shown in Fig. 9. As we can see, the two scenarios can be distinguished with high significance and statistics. The mass composition separation power can be enhanced by constructing a combined significance. Using the combination of all of the available observables, we should be able to reach 10% sensitivity for a proton fraction at the highest energies with more than  $5\sigma$  confidence level after 5 years of the AugerPrime operation (see the black line in Fig. 9).

## 7. Conclusions

AugerPrime, the ongoing upgrade of the Pierre Auger Observatory, has been designed to provide definitive answers to some of the pressing questions on UHECRs. It will enhance our ability to measure the mass composition of cosmic rays at energies above the flux suppression region and will allow for a superior separation of the muonic and electromagnetic components of air showers. As a part of the Upgrade, construction of the world-largest radio detector (covering an area of 3000 km<sup>2</sup>) has already started. Moreover, scintillator detectors installed on top of the surface detectors across the entire Observatory will enable a direct comparison of the Auger measurements with those of the surface detectors of the Telescope Array experiment.

The upgraded Observatory will be a multi-hybrid cosmic ray detector, that will allow simultaneous measurement of extensive air showers with water-Cherenkov, surface scintillator, radio, underground muon, and fluorescence detectors. Its capa-



bilities is illustrated in Fig. 10, where a real multi-hybrid event with the measured lateral signals of all the surface techniques is shown.

AugerPrime will help us to elucidate the origin of the UHECR flux suppression (to differentiate between the GZK or maximum rigidity scenario), to get information on primary mass composition on an event-by-event basis, to determine the proton flux contribution (as small as 10%) at the highest energies, and last but not least, to reduce systematic uncertainties related to modeling hadronic showers.

## Acknowledgments

The successful installation, commissioning, and operation of the Pierre Auger Observatory would not have been possible without the strong commitment and effort from the technical and administrative staff in Malargue, and the financial support from a number of funding agencies in the participating countries, listed at <https://www.auger.org/index.php/about-us/funding-agencies>. In particular we want to acknowledge support in Poland from National Science Centre grants No. 2016/23/B/ST9/01635 and No. 2020/39/B/ST9/01398, and also from Ministry of Science and Higher Education grant No. DIR/WK/2018/11.

## References

1. Pierre Auger Collaboration (A. Aab *et al.*), *Nucl. Instrum. Meth. A* **798**, 172 (2015), [arXiv:1502.01323 \[astro-ph.IM\]](#), doi:10.1016/j.nima.2015.06.058.
2. Pierre Auger Collaboration (J. Abraham *et al.*), *Nucl. Instrum. Meth. A* **613**, 29 (2010), [arXiv:1111.6764 \[astro-ph.IM\]](#), doi:10.1016/j.nima.2009.11.018.
3. Pierre Auger Collaboration (J. Abraham *et al.*), *Nuclear Instruments and Methods in Physics Research Section A: Accelerators, Spectrometers, Detectors and Associated Equipment* **620**, 227–251 (Aug 2010), doi:10.1016/j.nima.2010.04.023.
4. Pierre Auger Collaboration (A. Aab *et al.*), *Journal of Instrumentation* **11**, P02012 (Feb 2016), doi:10.1088/1748-0221/11/02/p02012.
5. Pierre Auger Collaboration (B. Daniel *et al.*), *Journal of Physics: Conference Series* **632**, 012088 (Aug 2015), doi:10.1088/1742-6596/632/1/012088.
6. Pierre Auger Collaboration (P. Abreu *et al.*), *Journal of Instrumentation* **7**, P11023 (Nov 2012), doi:10.1088/1748-0221/7/11/p11023.
7. Pierre Auger Collaboration (A. Aab *et al.*), *Phys. Rev. Lett.* **125**, 121106 (Sep 2020), doi:10.1103/PhysRevLett.125.121106.
8. Pierre Auger Collaboration (A. Aab *et al.*), *Journal of Cosmology and Astroparticle Physics* **08**, 049 (Aug 2015), doi:10.1088/1475-7516/2015/08/049.
9. Pierre Auger Collaboration (A. Aab *et al.*), *Science* **357**, 1266 (2017), <https://science.sciencemag.org/content/357/6357/1266.full.pdf>, doi:10.1126/science.aan4338.
10. Pierre Auger Collaboration (A. Aab *et al.*), *The Astrophysical Journal* **891**, 142 (Mar 2020), doi:10.3847/1538-4357/ab7236.
11. Pierre Auger Collaboration (A. Aab *et al.*), *Physical Review D* **91**, 032003 (Feb 2015), doi:10.1103/physrevd.91.032003.
12. Pierre Auger Collaboration (A. Aab *et al.*), *Physical Review Letters* **117**, 192001 (Oct 2016), doi:10.1103/physrevlett.117.192001.

13. Pierre Auger Collaboration (A. Aab *et al.*), *The European Physical Journal C* **80**, 751 (Aug 2020), doi:10.1140/epjc/s10052-020-8055-y.
14. D. Góra, Particle physics in cosmic rays, *International Journal of Modern Physics A*, proceedings of the 9th International Conference on New Frontiers in Physics 2020 (2021).
15. Pierre Auger Collaboration (A. Aab *et al.*), *Journal of Cosmology and Astroparticle Physics* **04**, 038 (Apr 2017), doi:10.1088/1475-7516/2017/04/038.
16. K. Greisen, *Phys. Rev. Lett.* **16**, 748 (Apr 1966), doi:10.1103/PhysRevLett.16.748.
17. G. T. Zatsepin and V. A. Kuzmin, *JETP Lett.* **4**, 78 (1966).
18. Pierre Auger Collaboration (A. Yushkov), *PoS ICRC2019*, 482 (2020), doi:10.22323/1.358.0482.
19. Pierre Auger Collaboration (J. Bellido), *PoS ICRC2017*, 506 (2018), doi:10.22323/1.301.0506.
20. Pierre Auger Collaboration (C. J. Todero Peixoto), *PoS ICRC2019*, 440 (2020), doi:10.22323/1.358.0440.
21. Pierre Auger Collaboration (A. Aab *et al.*), *Phys. Rev. D* **96**, 122003 (Dec 2017), doi:10.1103/PhysRevD.96.122003.
22. Pierre Auger Collaboration (A. Aab *et al.*), *Physics Letters B* **762**, 288–295 (Nov 2016), doi:10.1016/j.physletb.2016.09.039.
23. Pierre Auger Collaboration (A. Aab *et al.*), *Phys. Rev. D* **90**, 122006 (Dec 2014), doi:10.1103/PhysRevD.90.122006.
24. Pierre Auger Collaboration (A. Aab *et al.*), *Phys. Rev. D* **90**, 122005 (Dec 2014), doi:10.1103/physrevd.90.122005.
25. Pierre Auger Collaboration (P. Abreu *et al.*) (2011), [arXiv:1107.4804 \[astro-ph.HE\]](#).
26. Pierre Auger Collaboration (A. Aab *et al.*), *Journal of Cosmology and Astroparticle Physics* **10**, 022 (Oct 2019), doi:10.1088/1475-7516/2019/10/022.
27. Pierre Auger Collaboration (J. Abraham *et al.*), *Science* **318**, 938–943 (Nov 2007), doi:10.1126/science.1151124.
28. Pierre Auger Collaboration (P. Abreu *et al.*), *Astroparticle Physics* **34**, 314–326 (Dec 2010), doi:10.1016/j.astropartphys.2010.08.010.
29. Pierre Auger Collaboration (A. Aab *et al.*) (2016), [arXiv:1604.03637 \[astro-ph.IM\]](#).
30. Pierre Auger Collaboration (J. Pekala), *PoS ICRC2019*, 380 (2019).
31. Pierre Auger Collaboration (D. Nitz), *PoS ICRC2019*, 370 (2019).
32. F. G. Schröder, *Progress in Particle and Nuclear Physics* **93**, 1–68 (Mar 2017), doi:10.1016/j.pnpnp.2016.12.002.
33. Huege, Tim and on behalf of the Pierre Auger Collaboration, *EPJ Web Conf.* **210**, 05011 (2019), doi:10.1051/epjconf/201921005011.
34. T. Huege, M. Ludwig and C. W. James, *AIP Conf. Proc.* **1535**, 128 (2013), [arXiv:1301.2132 \[astro-ph.HE\]](#), doi:10.1063/1.4807534.
35. T. Huege and A. Haungs, *JPS Conf. Proc.* **9**, 010018 (2016), doi:10.7566/JPSCP.9.010018.
36. Pierre Auger Collaboration (A. Aab *et al.*), *Journal of Instrumentation* **12**, P03002 (Mar 2017), doi:10.1088/1748-0221/12/03/p03002.
37. Pierre Auger Collaboration (J. Abraham *et al.*), *Physical Review Letters* **104**, 091101 (Mar 2010), doi:10.1103/physrevlett.104.091101.
38. Pierre Auger Collaboration (P. Abreu *et al.*), *Journal of Cosmology and Astroparticle Physics* **02**, 026 (Feb 2013), doi:10.1088/1475-7516/2013/02/026.